

Supporting Information

Norfloxacin and Bisphenol-A Removal Using Temperature-Switchable Graphene

Oxide

Na Yao ^{†, #}, Xuntong Zhang ^{†, #}, Zhen Yang ^{†, ‡, *}, Weiben Yang ^{†, *}, Ziqi Tian[§], Limin

Zhang [†]

[†] School of Chemistry and Materials Science, Jiangsu Provincial Key Laboratory of Material Cycling and Pollution Control, Nanjing Normal University, Nanjing 210023, China

[‡] Changzhou Institute of Innovation & Development, Nanjing Normal University, Changzhou 213022, China

[§] Ningbo Institute of Materials Technology & Engineering, Chinese Academy of Sciences, Ningbo 315201, China

[#] Both authors contributed equally.

^{*} Corresponding authors.

E-mails: yangzhen@njnu.edu.cn (Zhen Yang), yangwb007@njnu.edu.cn (Weiben Yang)

Summary

Total pages: 32 (S-1 – S-32)

Text S1. Synthesis of P-GO. (S-4 – S-5)

Text S2. Characterization methodologies. (S-6 – S-7)

Text S3. Characterization results of P-GO. (S-8 – S-9)

Text S4. Calculation of adsorption capacity. (S-10)

Text S5. Density functional theory (DFT) calculation details. (S-11)

Text S6. Descriptions of adsorption kinetic models. (S-12)

Text S7. Representation of different isothermal adsorption equations. (S-13)

Text S8. Calculation method of theoretical adsorption amount in each cycle of adsorption-desorption. (S-14 – S-15)

Table S1. LCST values of different PNNPAM-COOH with different lengths. (S-16)

Table S2. Physico-chemical properties of NOR and BPA. (S-17)

Table S3. Kinetic parameters for the adsorption of NOR and BPA onto P-GO. (S-18)

Table S4. Isothermal parameters for the adsorption of NOR and BPA onto P-GO. (S-19)

Table S5. XPS peak normalization results of adsorbents before and after adsorption. (S-20)

Table S6. Theoretical and experimental values of adsorption amount of P-GO in each cycle of adsorption-desorption. (S-21)

Figure S1. Synthetic routes of PNNPAM-COOH (a); Transmittances at 500 nm of solutions containing PNNPAM-COOH with different chain length (b). (S-22)

Figure S2. FTIR patterns of GO, PNNPAM and P-GO. (S-23)

Figure S3. C1s XPS spectra of GO (a) and P-GO (b). (S-24)

Figure S4. Raman spectra of GO and PGO. (S-25)

Figure S5. TGA curves of GO and P-GO. (S-26)

Figure S6. ZP-pH profiles of GO and P-GO at 15 °C and 35 °C. (S-27)

Figure S7. H-bonds formed between PNNPAM and water molecules at 15 °C (a) and 35 °C (b). (PNNPAM and water molecules are separated for better illustration.) (S-28)

Figure S8. Adsorption kinetics (a and b) and adsorption isotherms (c and d) of NOR and BPA onto P-GO. (S-29)

Figure S9. Electrostatic potential surfaces: GO's computational models of sp^3 and sp^2 regions (a); PNNPAM (4 repeated units) (b); NOR (c) and BPA (d). (S-30)

References (S-31 – S-32)

Text S1. Synthesis of P-GO.

P-GO was synthesized according to the following route:

1. Preparation of GO

GO was synthesized by a modified Hummers' method.^{S1} Firstly, 230 mL of concentrated H₂SO₄ was added into a four-neck flask placed in ice-water bath. After 7 g of graphite and 5 g of NaNO₃ were slowly added, the suspension was stirred vigorously to prevent caking. Then, 30 g of KMnO₄ was carefully added into the flask (ensuring that the temperature was lower than 5 °C). The suspension was warmed slowly to 35 °C, and stirred for 120 min at this temperature. After this period, 400 mL of distilled water was added dropwisely, and the temperature increased rapidly to ~95°C. The mixture was refluxed at this temperature with continuous stirring for 25 min. Then, 50 mL of 30 wt.% H₂O₂ was added, in order to make the color of the mixture become light brown. The mixture was centrifuged. The solid was washed by 5 wt.% HCl solution and distilled water for three times, and finally dried at 60°C for 8 h.

2. Preparation of NNPAM^{S2}

Desired amounts of n-propylamine was firstly dissolved in 20 mL of toluene. Then, acryloyl chloride toluene solution (4 mL of acryloyl chloride in 15 mL of toluene) was added slowly at 5 °C for 1 h and subsequently at 10 °C for 30 min with continuous stirring. The mixture was filtrated to remove the resulting precipitate (n-propylamine hydrochloride). The filtrate was mixed with 50 mL of n-hexane, stirred for 5 min, and then allowed to separate into layers in ice-water bath. The lower layer (concentrated NNPAM solution) was collected and washed by 50mL of n-hexane. After rotary evaporation under 30 °C, NNPAM was obtained.

3. Preparation of PNNPAM-COOH^{S3}

Thiol acetic acid was dissolved in benzene in flask. After the solution was heated to 60 °C, nitrogen was introduced for 30 min to remove oxygen in the solution. After 2,2'-azoisobutyronitrile (AIBN) toluene solution was added into the flask, NNPAM tetrahydrofuran solution was added dropwisely, and polymerization reaction was carried out at 60 °C for 6 h under nitrogen atmosphere. PNNPAM-COOH was obtained by filtration in ethyl ether.

4. Grafting PNNPAM onto GO

0.5 g of PNNPAM-COOH was dissolved in ice-water and magnetic stirring in the ice-water bath, followed by adjusting pH to 8.0. After 0.1 g of N-hydroxysuccinimide (NHS) and 0.15 g 1-(3-dimethylaminopropyl)-3-ethylcarbodiimide hydrochloride (EDCI) as activating agents were dissolved in the reactor, the mixed solution was further stirred for 12h in the ice-water bath. Pulverous GO (0.5 g) was then added. The solution was kept in ice-water bath for 12h, and stirred for 5 h at room temperature. Then, the mixture was centrifuged. The obtained solid was washed by distilled water for three times and vacuum dried at 50 °C.

Text S2. Characterization methodologies.

Characterizations of the obtained P-GO include identification of chemical structure (by Fourier infrared spectroscopy (FTIR), X-ray photoelectron spectroscopy (XPS), Raman spectroscopy, X-ray diffraction (XRD) and thermogravimetric analysis (TGA)), observation of microscopic morphology (by atomic force microscope (AFM)), determination of temperature-responsiveness (by water contact angle (WCA) and molecular dynamics (MD) computation), surface-charge property (by Zeta potential (ZP)) and particle size distribution (PSD).

FTIR were recorded on a Bruker Tensor-27 FTIR spectrometer within a wavenumber range of 550-4000 cm^{-1} . XPS spectra were characterized on a ULVAC-PHI 5000 VersaProbe XPS spectrometer. Raman spectra were recorded on a LabRAM HR Horiba Jobin Yvon S.A.S. Raman spectrometer. XRD patterns were recorded on a Rigaku D/max 2500VL/PC X-ray diffractometer at a voltage of 40 kV and a current of 30 mA using Cu $K\alpha$ radiation. TGA curves was obtained on a Perkin-Elmer Pyris-1 TGA system in air atmosphere (the airflow rate is 30 cm^3/min) with a scanning rate of 10 $^{\circ}\text{C}/\text{min}$ from room temperature to 800 $^{\circ}\text{C}$. AFM measurements were performed using a Molecular Imaging PicoPlus AFM in an AC mode. LCST determination was performed using solution transmittance measurement method on a Hitachi UH5300 UV-vis spectrophotometer at a wavelength of 500 nm, with the PNNPAM-COOH concentration of 5.0 g/L. Water contact angles were measured using the sessile drop method with 3 μL water droplet and a Rame-Hart-100 telescopic goniometer. ZP was measured on a Malvern Nano-Z Zetasizer. Particle size distribution measurements were carried out on a Malvern Mastersizer-3000 light scattering system.

MD calculations were performed with LAMMPS Molecular Dynamics Simulator, using a model with non-periodic boundaries, to simulate structure of a PNNPAM molecular chain (21 repeated units) grafted on GO sheets in water solution (2000 H₂O molecules). Calculations were all based on Consistent Valence Forcefield (CVFF) for 3ns for each run. NVT (constant Number of particles, constant volume, and constant temperature) ensemble was used for each system, in which temperatures were controlled at 15 and 35 °C, respectively, to simulate practical environments of adsorption experiments.

Text S3. Characterization results of P-GO.

Fig. S2 shows FTIR spectra of GO, PNNPAM and P-GO. Peaks located from 2875 to 2964 cm^{-1} and the peak at 1149 cm^{-1} represent stretching and bending vibrations of n-propyls of PNNPAM and P-GO, which are not shown on the spectrum of GO. Meantime, the peak at 1642 cm^{-1} indicates the amide group of PNNPAM.^{S4} Fig. S3 shows XPS spectra (Normalized XPS peak areas listed in Table S5). Compared to the spectrum of GO, new peaks such as C-C, C-S, C-N and CO-NH are presented in Fig. S3b, demonstrating the existence of PNNPAM component. Normalized peak areas of C=C and C-O are drastically decreased (C=C: 0.4580 to 0.3773, C-O: 0.2801 to 0.1504), which means a large number of surface areas of GO, including sp^2 and sp^3 regions, are covered by the introduction of PNNPAM.^{S5} In Raman spectra (Fig. S4), two prominent peaks at 1358 and 1601 cm^{-1} correspond to the D band and G band for GO while the Raman spectrum of P-GO composites has bands at 1356 and 1595 cm^{-1} . The changed relative intensity of the D band indicates that the PNNPAM has interacted with the GO nanosheets rather than simply mixed. The I_D/I_G ratio is used to estimate the relative extent of structural defects. The values of I_D/I_G are 1.38 for GO nanosheets and 1.51 for P-GO composites, which indicates P-GO contains a lower percentage of the sp^2 regions and PNNPAM was successfully grafted onto GO sheets.^{S6} In TGA curves (Fig. S5), a three-step weight loss of GO nanosheets and P-GO composites is observed. The weight loss below 120 $^{\circ}\text{C}$ can be attributed to the evaporation of residual organic solvent and water. For GO nanosheets, the second significant weight loss is observed from 130 to 230 $^{\circ}\text{C}$ (~35% weight loss), which is related to the loss of CO and/or CO_2 from the decomposition of oxygen-containing functional groups; The third weight loss at the temperature range from 460 to 600 $^{\circ}\text{C}$ is attributed to the complete combustion of the carbon backbones

of graphene. For P-GO, the second weight loss is found from 120 to 240 °C (~23% weight loss) owing to the decomposition of GO nanosheets;^{S7} The third large weight loss occurred at temperature up to 600 °C is mainly due to the decomposition of the backbones of graphene and PNNPAM polymers. Considering the weight loss of moisture (~10% weight loss) in the sample, the weight percentage of PNNPAM polymers grafted in dry P-GO is calculated to be ~20%. Surface charge properties of adsorbents are investigated by ZP-pH profiles in Fig. S6. Both GO and P-GO have negatively charged surface in the whole tested pH range

Text S4. Calculation of adsorption capacity.

The adsorption capacity, Q_e (mg/g), is calculated by

$$Q_e = (C_0 - C_e)V/m \quad (\text{Eq. S1})$$

where C_0 and C_e (mg/L) is the initial and final contaminant concentrations, V (L) is the volume of solution, and m (g) is the mass of adsorbent.

Text S5. Density functional theory (DFT) calculation details.^{S8}

A finite 14-membered carbon ring model was chosen for graphene oxide by comprehensive considering computational cost and accuracy.^{S9-S12} Theoretical calculation is performed using B3LYP hybrid function of DFT calculations. The M06-2x/6-31+G (d) basis set method is employed to optimize geometries of representative functional groups of P-GO, EOCs and their complexes. Strengths of interactions between P-GO and EOCs are evaluated by absolute value of binding energy (BE):

$$BE = |E_{\text{complex(P-GO-EOC)}} - E_{\text{P-GO}} - E_{\text{EOC}}| \quad (\text{Eq. S2})$$

where $E_{\text{complex(P-GO-EOC)}}$, $E_{\text{P-GO}}$ and E_{EOCs} were energies of optimized geometries of complex, representative functional groups of P-GO, and EOCs, respectively

Text S6. Descriptions of adsorption kinetic models.

The pseudo-first order model assumes that the sorption rate decreases linearly with the increase of adsorption capacity. The pseudo-first order model is given as

$$\ln(Q_e - Q_t) = \ln Q_e - k_1 t \quad (\text{Eq. S3})$$

where Q_e and Q_t (mg/g) are the amounts of the contaminant onto the adsorbents at equilibrium and at time t (min). k_1 (min^{-1}) is the rate constant in the pseudo-first order adsorption model.

The pseudo-second order kinetic model assumes that the rate-limiting step is the interaction between two reagent particles. It is usually used to describe a chemical adsorption. Its linear form is

$$\frac{t}{Q_t} = \frac{1}{k_2 Q_e^2} + \frac{t}{Q_e} \quad (\text{Eq. S4})$$

where k_2 ($\text{g}/(\text{mg} \cdot \text{min})$) is the rate constant in the pseudo-second order adsorption model.

Text S7. Representation of different isothermal adsorption equations.

The Langmuir isotherm model is on the basis of the assumption of identical sorption heat and monolayer sorption. The linear form of Langmuir equation is as follows:

$$\frac{C_e}{Q_e} = \frac{1}{Q_L b} + \left(\frac{1}{Q_L}\right) C_e \quad (\text{Eq. S5})$$

where Q_e (mg/g) is the adsorption capacity, C_e (mg/L) is the equilibrium contaminant concentrations in water, Q_L (mg/g) is the theoretical saturate adsorption capacity in the Langmuir model, and b (L/mg) is the Langmuir isotherm constant demonstrating the tendency of adsorption.

The Freundlich model is an empirical model for a heterogeneous system. It expresses reversible sorption and is not restricted to the formation of the monolayer. The Freundlich model in linear form is

$$\ln Q_e = \ln K_F + \frac{\ln C_e}{n} \quad (\text{Eq. S6})$$

where K_F is the Freundlich isotherm constant and n is the heterogeneity factor.

Text S8. Calculation method of theoretical adsorption amount in each cycle of adsorption-desorption.

According to isotherm study results in the work, Langmuir model is suitable to describe the adsorption equilibrium data. Therefore, theoretical adsorption amount of P-GO after adsorption in each cycle could be calculated based on Langmuir model.

The following method takes adsorption/desorption of NOR as an example. Similar method can be used for BPA.

Firstly, use $Q_{e,i}$ (mg/g) and $C_{e,i}$ (mg/L) to represent the amount of the contaminant in P-GO and the concentration of the contaminant in water, respectively, after adsorption equilibrium is reached in **Cycle i**; use $Q'_{e,i}$ (mg/g) and $C'_{e,i}$ (mg/L) to represent the amount of the contaminant in P-GO and the concentration of the contaminant in water, respectively, after desorption equilibrium is reached in **Cycle i**. The adsorption-desorption cycles start with Cycle 0.

For desorption of NOR at 35 °C, according to fitting results in SI Table S4, the Langmuir relationship between $Q'_{e,i}$ and $C'_{e,i}$ could be written as

$$\frac{C'_{e,i}}{Q'_{e,i}} = \frac{1}{233.6 \times 0.0104} + \left(\frac{1}{233.6}\right) C'_{e,i} \quad (\text{Eq. S7})$$

According to mass conservation of the contaminant,

$$C'_{e,i} V + m Q'_{e,i} = m Q_{e,i} \quad (\text{Eq. S8})$$

where V is the volume of water used for desorption (0.009 L) and m is the mass of P-GO (0.010 g).

For adsorption of NOR at 15 °C, according to fitting results in SI Table S4, the Langmuir relationship between $Q_{e,i}$ and $C_{e,i}$ could be written as

$$\frac{C_{e,i}}{Q_{e,i}} = \frac{1}{243.3 \times 0.0539} + \left(\frac{1}{243.3}\right) C_{e,i} \quad (\text{Eq. S9})$$

According to mass conservation of the contaminant,

$$C_{e,i}V + mQ_{e,i} = mQ'_{e,i-1} + C_0V \quad (\text{Eq. S10})$$

where V is the volume of water used for adsorption (0.009 L) and C_0 is the initial concentration of the contaminant (200 mg/L for NOR).

For desorption in Cycle 0, $Q_{e,i}$ in Eq.(S8) is replaced by $Q_{e,0}$ (147 mg/g). Using Eqs. (S7 and S8), $Q'_{e,0}$ and $C'_{e,0}$ can be obtained; Then, for adsorption in Cycle 1, take $Q'_{e,0}$ into Eq. (S10), $Q_{e,1}$ and $C_{e,1}$ can be calculated using Eqs. (S9 and S10); Similarly, $Q'_{e,i}$, $C'_{e,i}$, $Q_{e,i}$ and $C_{e,i}$ in Cycle i can be calculated in turn. Finally, the apparent adsorption capacity in Cycle i (theoretical adsorption amount, mg/g), i.e. the newly adsorbed NOR in adsorption except the residual in P-GO after regeneration, is obtained by

$$\text{Theoretical adsorption amount} = Q_{e,i} - Q'_{e,i-1} \quad (\text{Eq. S11})$$

Table S1. LCST values of different PNNPAM-COOH with different lengths.

Sample name	P27	P21	P17
Monomer : Thiol acetic acid	30:1	25:1	20:1
Average repeated unit number (determined by end-group titration)	27	21	17
LCST (°C)	16	21	26

Table S2. Physico-chemical properties of NOR and BPA.

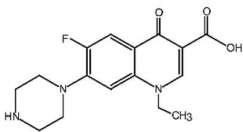
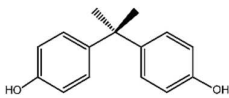
Contaminants	NOR	BPA
Molecular structure		
Molecular formula	$C_{16}H_{18}FN_3O_3$	$C_{15}H_{16}O_2$
Molecular weight (g/mol)	319.33	228.29
$pK_{a,1}$	6.22	9.78
$pK_{a,2}$	8.51	10.39
$\log K_{ow}$	-1.70	3.32

Table S3. Kinetic parameters for the adsorption of NOR and BPA onto P-GO.

Contaminants	Temperature	Pseudo-first order			Pseudo-second order		
		Q_{e1}	K_1	R^2	Q_{e2}	K_2	R^2
		(mg/g)	(min ⁻¹)		(mg/g)	(g/(mg·min))	
BPA	15 °C	22.2	0.170	0.922	23.4	0.01246	0.980
	35 °C	33.1	0.083	0.865	35.2	0.00382	0.926
NOR	15 °C	136.6	0.147	0.927	142.5	0.00405	0.972
	35 °C	87.8	0.105	0.894	93.7	0.00256	0.970

Table S4. Isothermal parameters for the adsorption of NOR and BPA onto P-GO.

Contaminants	Temperature	Langmuir model			Freundlich model		
		Q_L	b	R^2	K_F	n	R^2
		(mg/g)	(L/mg)		($\text{mg}^{1-n} \cdot \text{L}^n \cdot \text{g}^{-1}$)		
BPA	15 °C	46.7	0.0258	0.994	5.03	2.42	0.983
	35 °C	53.1	0.0633	0.991	12.2	3.41	0.971
NOR	15 °C	243.3	0.0539	0.984	68.1	4.28	0.957
	35 °C	233.6	0.0104	0.996	16.2	2.32	0.982

Table S5. XPS peak normalization results of adsorbents before and after adsorption.

Normalized peak areas									
Groups	C-C	C=C	C-S	C-N	C-O	C=O	C-F	CONH	O=C-O
GO	--	0.4580	--	--	0.2801	0.1480	--	--	0.1139
P-GO	0.2344	0.3773	0.0149	0.0640	0.1504	0.0409	--	0.0640	0.0542
P-GO-NOR	0.1415	0.1514	--	0.3774	0.2175	0.0167	0.0668	0.0123	0.0163
P-GO-BPA	0.1593	0.3596	--	0.0163	0.3974	0.0329	--	0.0145	0.0200

Table S6. Theoretical and experimental values of adsorption amount of P-GO in each cycle of adsorption-desorption.

Cycles	NOR (Adsorption amount (mg/g))		BPA (Adsorption amount (mg/g))	
	Theoretical value	Experimental value	Theoretical value	Experimental value
0	--	147.26	--	43.20
1	106.60	135.83	24.50	30.41
2	120.33	123.54	30.64	30.64
3	115.65	121.96	28.47	30.13
4	117.25	119.06	29.15	29.83
5	116.70	117.12	28.98	28.97
6	116.92	118.20	29.04	29.70
7	116.75	119.17	29.02	29.42
8	116.87	118.94	29.02	29.23

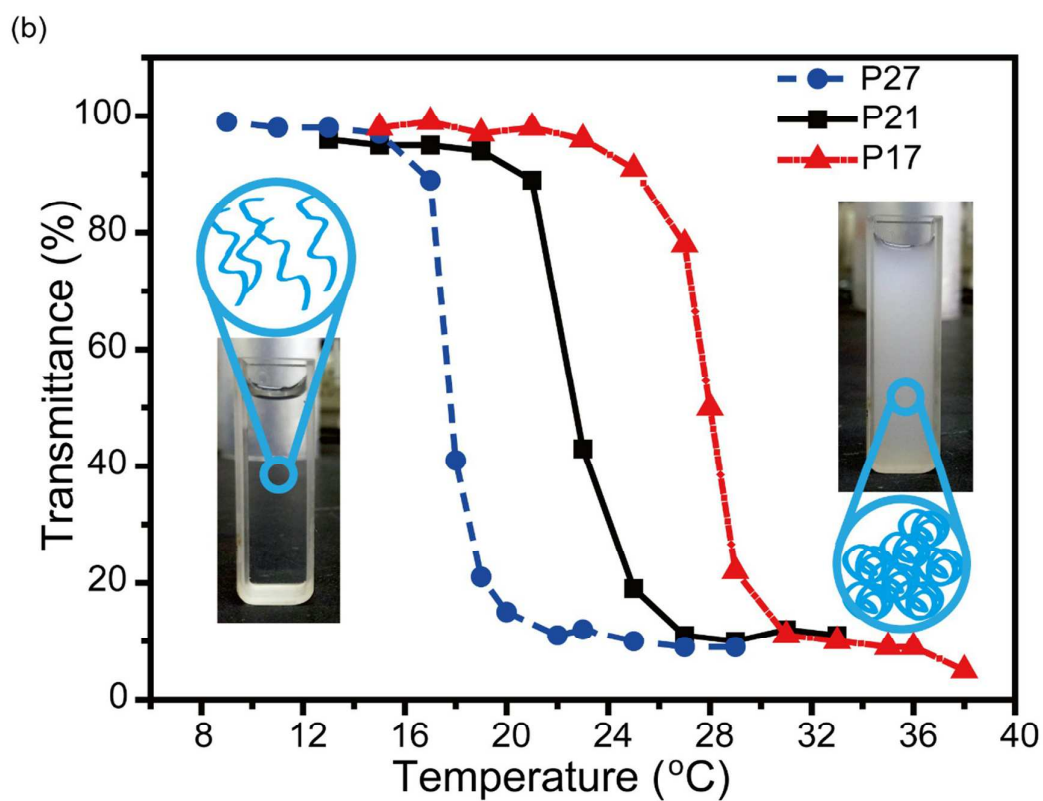
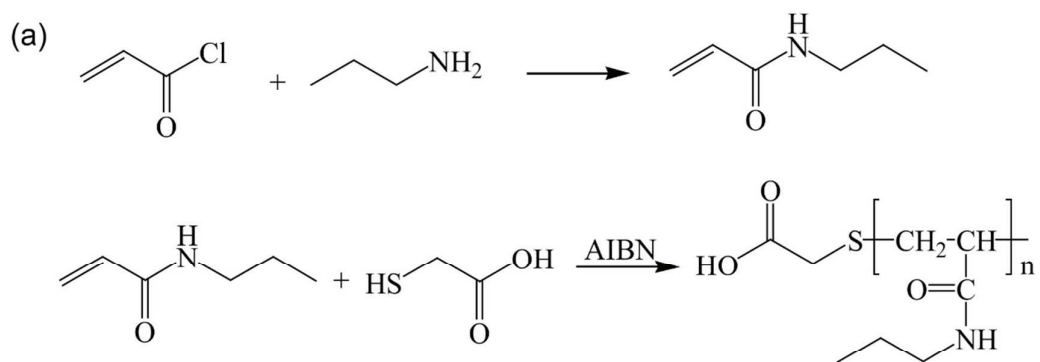


Figure S1. Synthetic routes of PNNPAM-COOH (a); Transmittances at 500 nm of solutions containing PNNPAM-COOH with different chain length (b).

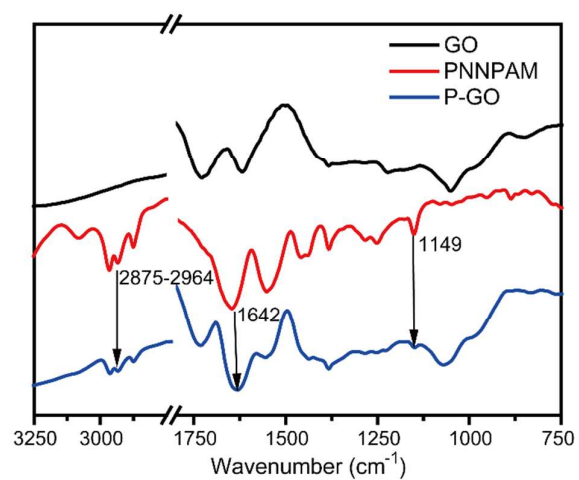


Figure S2. FTIR patterns of GO, PNNPAM and P-GO.

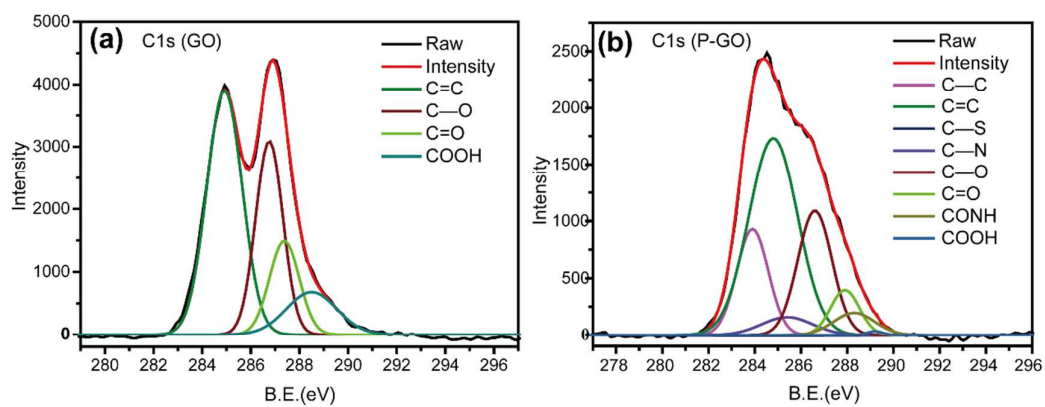


Figure S3. C1s XPS spectra of GO (a) and P-GO (b).

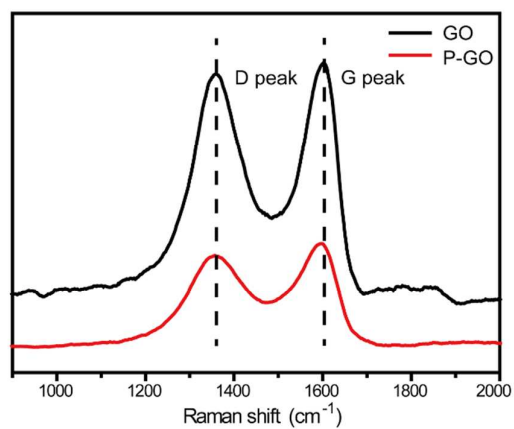


Figure S4. Raman spectra of GO and PGO.

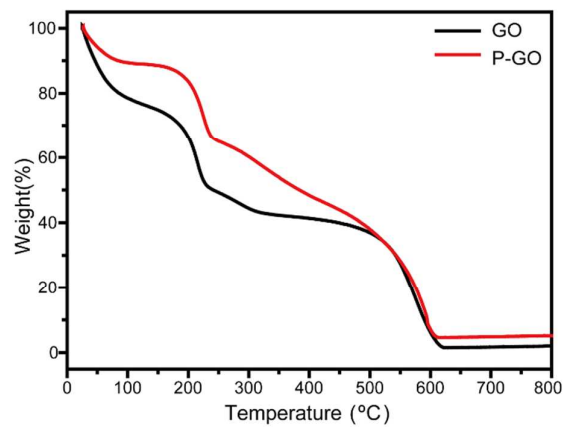


Figure S5. TGA curves of GO and P-GO.

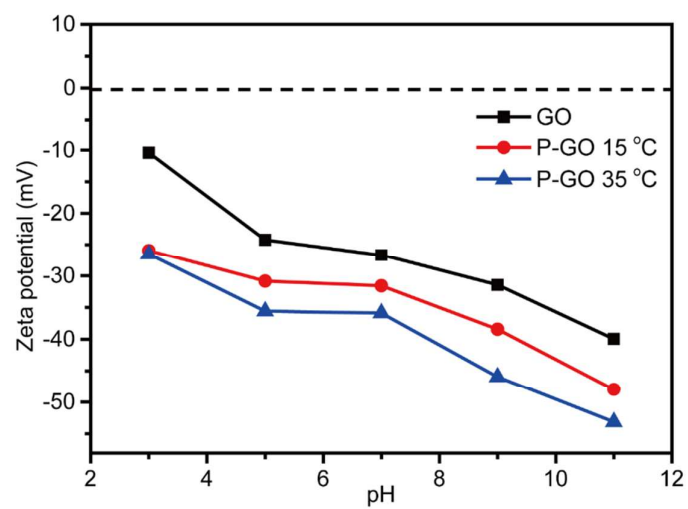


Figure S6. ZP-pH profiles of GO and P-GO at 15 °C and 35 °C.

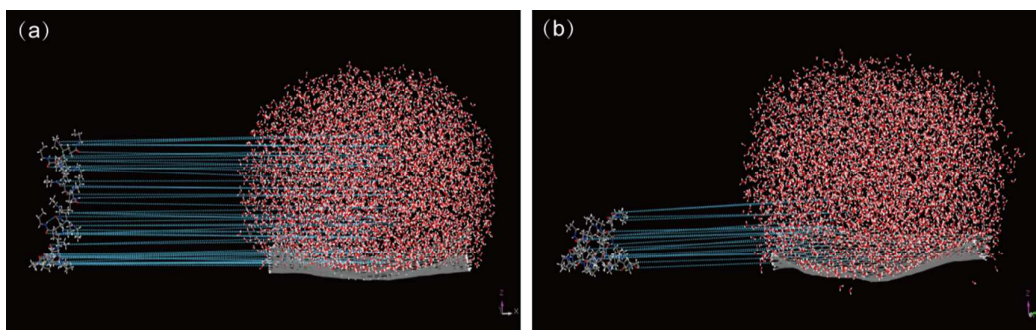


Figure S7. H-bonds formed between PNNPAM and water molecules at 15 °C (a) and 35 °C (b). (PNNPAM and water molecules are separated for better illustration.)

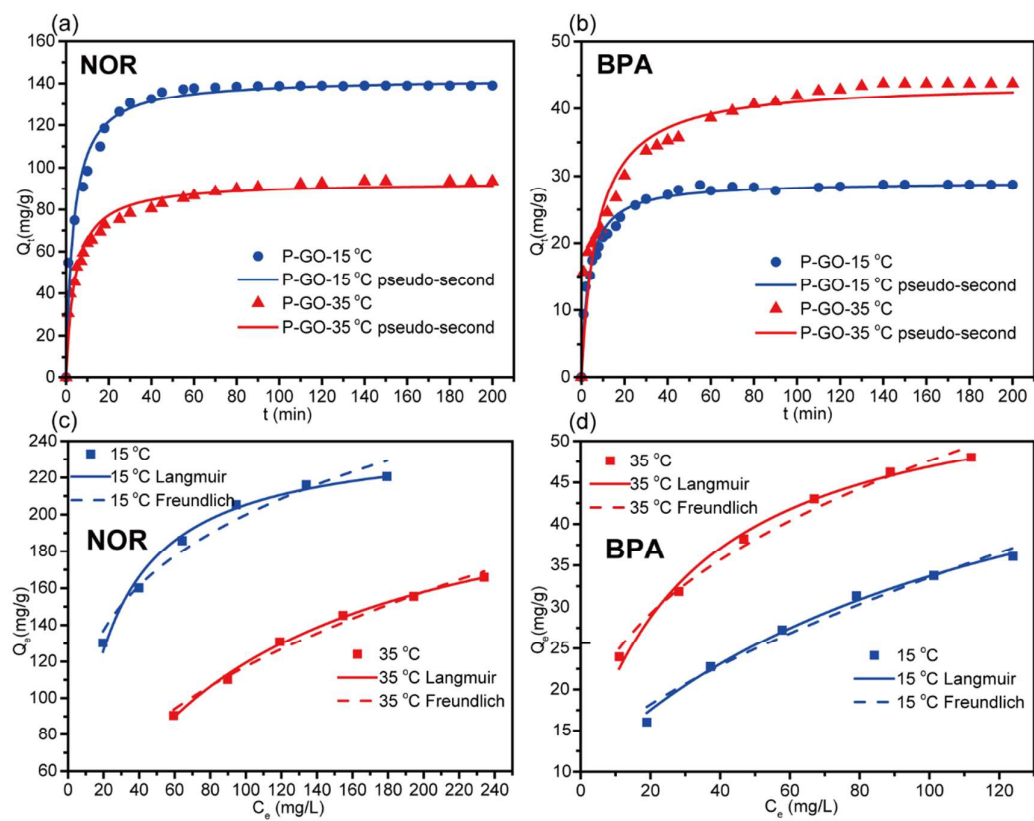


Figure S8. Adsorption kinetics (a and b) and adsorption isotherms (c and d) of NOR and BPA onto P-GO.

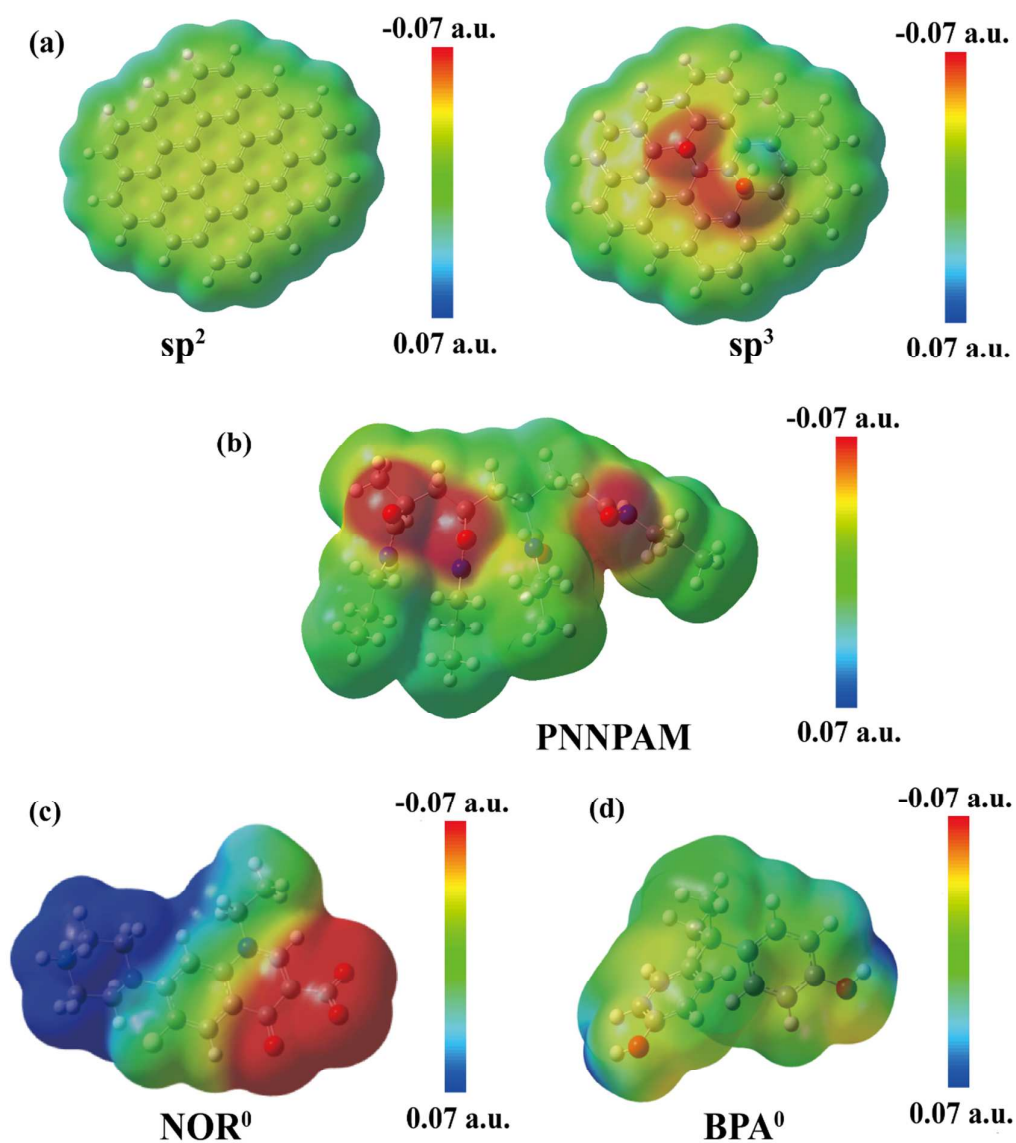


Figure S9. Electrostatic potential surfaces: GO's computational models of sp^3 and sp^2 regions (a); PNNPAM (4 repeated units) (b); NOR (c) and BPA (d).

References

- (S1) Jr, W. S. H.; Offeman, R. E. Preparation of Graphitic Oxide. *J. Am. Chem. Soc.* **1958**, *80*, 1339-1339.
- (S2) Chen, G.; Hoffman, A. S. Preparation and Properties of Thermoreversible, Phase-Separating Enzyme-Oligo(N-isopropylacrylamide) Conjugates. *Bioconjugate Chem.* **1993**, *4*, 509-514.
- (S3) Takei, Y. G.; Aoki, T.; Sanui, K.; Ogata, N.; Sakurai, Y.; Okano, T.; Matsukata, M.; Kikuchi, A. Temperature-Responsive Bioconjugates. 3. Antibody-Poly(N-isopropylacrylamide) Conjugates for Temperature-Modulated Precipitations and Affinity Bioseparations. *Bioconjugate Chem.* **1994**, *5*, 25-28.
- (S4) Wang, Z.; Lai, H.; Wu, P. Influence of PIL Segment on Solution Properties of poly(N-isopropylacrylamide)-b-poly(Ionic Liquid) Copolymer: Micelles, Thermal Phase Behavior and Microdynamics. *Soft Matter* **2012**, *8*, 11644-11653.
- (S5) Jiang, L.; Messing, M. E.; Ye, L. Temperature and pH Dual-Responsive Core-Brush Nanocomposite for Enrichment of Glycoproteins. *ACS Appl. Mater. Interfaces* **2017**, *9*, 8985-8995.
- (S6) Song, W.; Wang, X.; Wang, Q.; Shao, D.; Wang, X. Plasma-Induced Grafting of Polyacrylamide on Graphene Oxide Nanosheets for Simultaneous Removal of Radionuclides. *Phys. Chem. Chem. Phys.* **2015**, *17*, 398-406.
- (S7) Hu, R.; Shao, D.; Wang, X. Graphene Oxide/Polypyrrole Composites for Highly Selective Enrichment of U(VI) from Aqueous Solutions. *Polym. Chem.* **2014**, *5*, 6207-6215.
- (S8) Frisch, M. J., Trucks, G. W., Schlegel, H. B., Scuseria, G. E., Robb, M. A., Cheeseman, J. R., Scalmani, G., Barone, V., Petersson, G. A., Nakatsuji, H., Li, X., Caricato, M., Marenich, A., Bloino, J., Janesko, B. G., Gomperts, R., Mennucci, B.,

Hratchian, H. P., Ortiz, J. V., Izmaylov, A. F., Sonnenberg, J. L., Williams-Young, D., Ding, F., Lipparini, F., Egidi, F., Goings, J., Peng, B., Petrone, A., Henderson, T., Ranasinghe, D., Zakrzewski, V. G., Gao, J., Rega, N., Zheng, G., Liang, W., Hada, M., Ehara, M., Toyota, K., Fukuda, R., Hasegawa, J., Ishida, M., Nakajima, T., Honda, Y., Kitao, O., Nakai, H., Vreven, T., Throssel, K., Montgomery, J. A., Jr, Peralta, J. E., Ogliaro, F., Bearpark, M., Heyd, J. J., Brothers, E., Kudin, K. N., Staroverov, V. N., Keith, T., Kobayashi, R., Normand, J., Raghavachari, K., Rendell, A., Burant, J. C., Iyengar, S. S., Tomasi, J., Cossi, M., Millam, J. M., Klene, M., Adamo, C., Cammi, R., Ochterski, J. W., Martin, R. L., Morokuma, K., Farkas, O., Foresman, J. B., and Fox, D. J., Gaussian, Inc., Wallingford CT, **2016**.

(S9) Ai, Y. J.; Liu, Y.; Lan, W. Y.; Jin, J. R.; Xing, J. L.; Zou, Y. D.; Zhao, C. F.; Wang, X. K., The Effect of pH on the U(VI) Sorption on Graphene Oxide (GO): A Theoretical Study. *Chem. Eng. J.* **2018**, *343*, 460-466.

(S10) Jin, Z.; Wang, X.; Sun, Y.; Ai, Y.; Wang, X. Adsorption of 4-n-Nonylphenol and Bisphenol-A on Magnetic Reduced Graphene Oxides: A Combined Experimental and Theoretical Studies. *Environ. Sci. Technol.* **2015**, *49*, (15), 9168-9175.

(S11) Wang, X.; Liu, Y.; Pang, H.; Yu, S.; Ai, Y.; Ma, X.; Song, G.; Hayat, T.; Alsaedi, A.; Wang, X., Effect of Graphene Oxide Surface Modification on the Elimination of Co(II) from Aqueous Solutions. *Chem. Eng. J.* **2018**, *344*, 380-390.

(S12) Zhang, X.; Shen, J.; Zhuo, N.; Tian, Z.; Xu, P.; Yang, Z.; Yang, W. Interactions between Antibiotics and Graphene-Based Materials in Water: A Comparative Experimental and Theoretical Investigation. *ACS Appl. Mater. Interfaces* **2016**, *8*, (36), 24273-24280.